# ACCEPTED VERSION

http://hdl.handle.net/2440/133332

# Physiological response of the retinal pigmented epithelium to 3-ns pulse laser application, in vitro and in vivo

John P. M. Wood DPhil[1,2]  |  Marzieh Tahmasebi MBBS[1,2]  |
Robert J. Casson DPhil FRANZCO[1,2]  |  Malcolm Plunkett[2]  |  Glyn Chidlow DPhil[1,2]

[1]Central Adelaide Local Health Network, Adelaide, South Australia, Australia

[2]Discipline of Ophthalmology and Visual Sciences, University of Adelaide, Adelaide, South Australia, Australia

Correspondence
John P. M. Wood, DPhil, Ophthalmic Research Laboratories, Level 7, Adelaide Health and Medical Sciences Building, North Terrace, Adelaide SA-5000, Australia.
Email: john.wood2@sa.gov.au

Abstract

Background: To treat healthy retinal pigmented epithelium (RPE) with the 3-ns retinal rejuvenation therapy (2RT) laser and to investigate the subsequent wound-healing response of these cells.

Methods: Primary rat RPE cells were treated with the 2RT laser at a range of energy settings. Treated cells were fixed up to 7 days post-irradiation and assessed for expression of proteins associated with wound-healing. For in vivo treatments, eyes of Dark Agouti rats were exposed to laser and tissues collected up to 7 days post-irradiation. Isolated wholemount RPE preparations were examined for structural and protein expression changes.

Results: Cultured RPE cells were ablated by 2RT laser in an energy-dependent manner. In all cases, the RPE cell layer repopulated completely within 7 days. Replenishment of RPE cells was associated with expression of the heat shock protein, Hsp27, the intermediate filament proteins, vimentin and nestin, and the cell cycle-associated protein, cyclin D1. Cellular tight junctions were lost in lased regions but re-expressed when cell replenishment was complete. In vivo, 2RT treatment gave rise to both an energy-dependent localised denudation of the RPE and the subsequent repopulation of lesion sites. Cell replenishment was associated with the increased expression of cyclin D1, vimentin and the heat shock proteins Hsp27 and αB-crystallin.

Conclusions: The 2RT laser was able to target the RPE both in vitro and in vivo, causing debridement of the cells and the consequent stimulation of a wound-healing response leading to layer reformation.

KEYWOR DS
nanosecond laser, retinal cell culture, retinal pigment epithelium, retinal rejuvenation therapy (2RT)

# 1 | INTRODUCTION

The retinal pigment epithelium (RPE) comprises a mono- layer of polygonal epithelial cells which are associated at their basal surface with Bruch's membrane and the choriocapillaries, and at their apical face with the outer segments of the photoreceptors, with which they inter- digitate.[1,2] RPE cells have many specialised functions in support of the homeostasis of the retina and dysfunction or loss of these cells will have profound effects on this tissue.[1,2] RPE cells are thought, for example, to be central to the pathogenesis of age-related macular degeneration (AMD): the accumulation of intracellular lipofuscin and deposits such as drusen underneath these cells are believed to cause cellular dysfunction, increased oxidative stress, and restricted flow of nutrients to the retina, thus contributing to outer retinal pathology.[1,3]

There is increasing evidence that in response to stress or trauma the RPE is able to undertake a wound-healing response.[4,5] During this process, RPE cells alter expression of membrane transporters,[6] matrix metalloproteinases (MMPs),[7] intermediate filaments and small heat shock proteins,[8] and other secretable factors.[9,10] These changes influence quiescent RPE cells to remodel Bruch's mem- brane and re-populate lesion sites allowing restoration of physiological retinal functioning.[1,7] Studies have con- firmed the participation of the RPE in tissue remodelling subsequent to trauma, choroidal rupture, sub-retinal neovascularisation and retinal detachment.[11-13] It has been postulated that the stimulation of a wound-healing response in diseases in which RPE cells are themselves dysfunctional could prove beneficial to improving retinal function.[11]

Interestingly, an RPE wound-healing response has been detected subsequent to laser photocoagulation,[12,14] in which thermal burns are applied to the retina to amelio- rate pathology associated with diseases such as diabetic macular edema (DME), wet AMD and proliferative dia- betic retinopathy. Although different mechanisms for the positive action of this therapy have been postulated,[15] it is now thought that the major beneficial effects derive from the RPE. This is because treatment is typically performed with green lasers that are only minimally absorbed by the macular pigment xanthophyll but strongly absorbed by the pigment-bearing melanosomes of the RPE.[16,17] Even at very low energy settings, however, experimental studies have indicated that the RPE and the overlying photorecep- tors are destroyed by photocoagulation,[16,18,19] with obvi- ous visual consequences.

Crucially, recent studies have shown that it is actually possible to both selectively target the RPE with laser pho- tocoagulation and to confine thermal energy within this cell layer, thus avoiding collateral damage to the retina or choroid.[20,21] Selective RPE targeting is a highly desir- able concept in the provision of therapy for AMD because it could theoretically be applied to the central macula. This principle has been applied to systems such as the selective retinal therapy (SRT)[5,20,22-24] and the retinal rejuvenation therapy (2RT) lasers.[21,25-27]

The 2RT laser is a recently-described system, which selectively targets the RPE by virtue of having a concise 3 ns pulse duration.[21,25-27] As a consequence, this laser will ablate some or all of the RPE cells within the irradiated zone and leave surrounding tissues intact. Studies have demonstrated in rodents that the 2RT laser does not cause a breach in Bruch's membrane and that there is no disruption to retinal neurons or photorecep- tors at clinically relevant energy settings.[8,19,28] It has also been shown that the 2RT laser induces release of acti- vated MMPs[7] and pigment epithelial-derived factor (PEDF)[29] as well as proliferation of local RPE cells and re-tiling of this cell layer.[28,30] Theoretically, the stimula- tion of such a response would be an ideal means to treat AMD, as it would revitalise the RPE cell layer, clear accu- mulated deposits from Bruch's membrane via MMP action and consequently relax any restriction in nutrient passage. Indeed, clinical testing has revealed that the 2RT laser does show promise in decreasing drusen and slowing the rate of progression in AMD patients.[27,30,31] These findings could be crucial for patients suffering from the non-exudative form of AMD, for which there is no current recognised treatment.

Since 2RT-induced RPE ablation has been previously documented, we sought to investigate the reaction of healthy cells to this laser, as a means to further under- stand the mechanisms by which this treatment could potentially address retinal disease treatment.

# 2 | METHODS

## 2.1 | Laser system

The 2RT system used was a frequency-doubled Nd:YAG laser with a 532 nm wavelength, a 3 ns pulse duration and a fine speckle-beam profile (Ellex R&D Pty Ltd, Ade- laide, South Australia). This laser has a 380 μm spot size in air and a spot size of 285 μm when focussed on the ret- ina; focussing was achieved using a 5.4 mm fundus laser contact lens (Ocular Instruments, Bellevue, WA). The laser was used at four distinct energy settings, which were each defined based on in vivo rat eye studies: 24, 64, 91 and 145 mJ/cm$^2$; only the latter two energy settings were used in the in vivo studies.

An explanation of the selection of these energy values is provided as Supporting Information.

## 2.2 | Primary rat RPE cell cultures

RPE cell cultures from rat were selected so that comple- mentary rat in vivo studies could be performed. Dark Agouti rats were selected because these animals are pigmented and because a supply was readily available to us. All medium and culture additives were obtained from ThermoFisher Scientific (Adelaide, SA, Australia), except
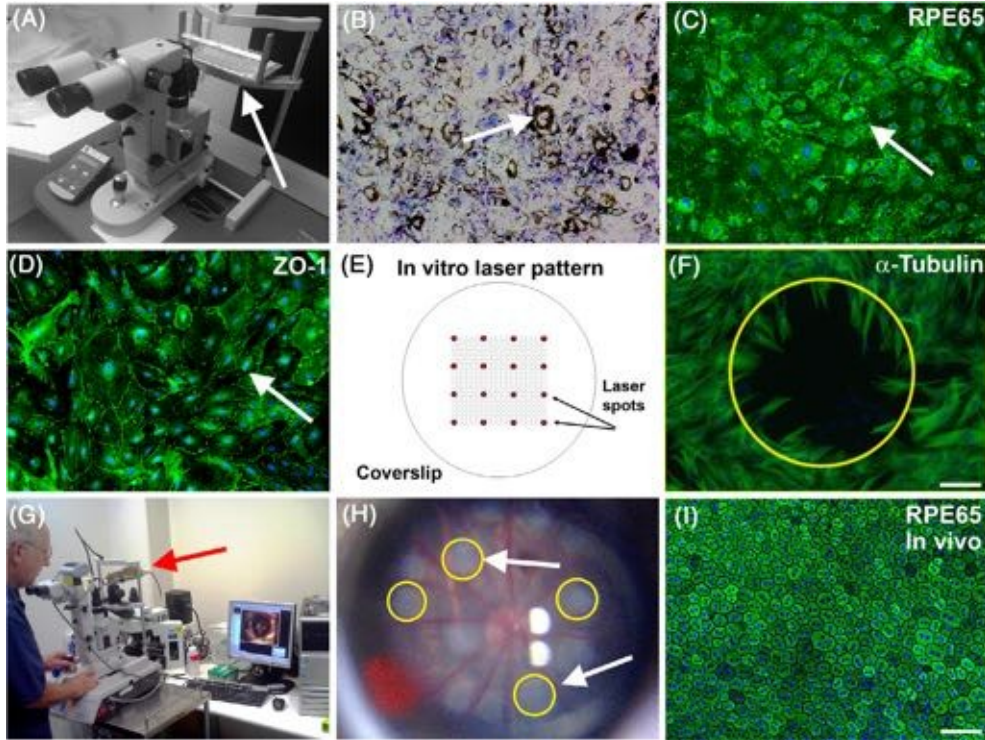


**FIGURE 1** Methodological considerations for analysis of the retinal pigmented epithelium (RPE) in vitro (A–F) and in vivo (G–I). (A) Treatment of cells in vitro was undertaken in culture plates exposed to laser on a horizontal platform (arrow) attached to a slit-lamp headrest. (B) Appearance of untreated RPE cells in culture after labelling with haematoxylin, showing presence of intracellular pigment (e.g., arrow). (C) Immunocytochemical labelling of cells at passage number 1 with the RPE-specific protein RPE65, showing cytoplasmic labelling (arrow) and demonstrating specificity and homogeneity of the cultures. (D) Immunocytochemical labelling of cultured cells at passage number 1 with ZO-1, showing labelling of cell peripheries (arrow) demonstrating presence of intact tight junctions. (E) Schematic image demonstrating pattern of laser irradiation on coverslip: 16 spots were applied (red circles) in a 4 ✕ 4 grid with approximately 5 spot widths between each application (white circles). (F) RPE cells fixed immediately after application of 2RT laser (91 mJ/cm$^2$), showing position of lased region (yellow circle) and resultant lesion area (cells labelled for α-tubulin). (G) Treatment of rat retina/RPE in vivo; operator places anaesthetised rat on bespoke holder attached to patient headrest (red arrow) and laser is applied via slit-lamp delivery system linked to a monitor. (H) Illustration of laser application to rat eye via fundus imaging; yellow circles show the position of lased regions as visible blanching in the pigmented layer. (I) Preparation of RPE wholemounts from untreated eyes labelled for RPE65, showing that cells are confluent and predominantly bi- or multi-nucleate. Cells shown in (C, D, E, F, I) have nuclei counter-labelled with DAPI (blue). Scale bars: (B–F, I) = 100 μm

where otherwise stated. RPE cultures were established from 10-12 day old Dark Agouti rat pups with a proce- dure based on that of Mayerson et al[32] and detailed in the Supporting Information section. Cultures were established from rat pup eyes because RPE cells from this source are known to establish readily, rather than those from adult animals.[32] Primary cultures were allowed to grow in growth medium: Minimal Essential Medium (MEM) containing 20% (v/v) foetal bovine serum, 2 mM L-glutamine (Sigma-Aldrich) and kanamycin/gen-

tamicin, for 7-10 days in a normal incubator at 37°C, 5%

$CO_2$ and saturating humidity. Sub-passaging was under- taken into flasks or onto sterile borosilicate glass cover- slips, at a ratio of 1:3, using growth medium containing 10% (v/v) foetal bovine serum. All investigations were carried out at first or second passage. Whilst the extent of

melanisation showed some variation at this stage, all cells retained some degree of pigment, ensuring laser targeting.

## 2.3 | Treatment of cells in culture

For laser treatment, confluent cells were treated on glass coverslips, in order to allow subsequent immunocyto- chemical labelling. Cells were transferred to wells in a

24 well-plate containing medium that was warmed to 37°C and was equivalent to normal growth medium except that it lacked phenol red indicator and had only 1% (v/v) foetal bovine serum. Culture plates were then placed on a height-adjustable bespoke horizontal platform attached to the slit-lamp patient chin rest (Figure 1(A)),

on which cells were treated. Laser light was directed and focussed onto the surface of the RPE cell layer in the wells via a 45° mirror fixed above the platform on which the cell plate was positioned. Energy loss from the mirror used to direct the laser onto cells was determined to be negligi- ble.[21] Each coverslip was exposed to 16 laser irradiations
in a 4x4 grid pattern with approximately 5 beam widths distant from any other in the X-Y plane (Figure 1(E)). Use of this grid allowed identification of lased zones in labelled coverslips, even if cells had re-populated the region. Treated cells were fixed at the appropriate times with 10% (w/v) neutral buffered formalin (NBF), containing 1% (v/v) methanol for 15 minutes. Some coverslips were dipped for 30 s in 10% haematoxylin to visualise culture appearance (Figure 1(B)).

It must be noted that, unlike humans, pigmented Dark-Agouti rats have a relatively uniform pigment level with little obvious difference between individuals and therefore energy range finding for each animal was con- sidered unnecessary. It is also important to note that although laser settings were defined on threshold values obtained from in vivo studies, the same settings were used for the in vitro work, even though, obviously, the treatment characteristics (e.g., light path, medium, level of cell pigmentation, etc.) would have differed. This was purely for consistency.

## 2.4 | Immunocytochemical labelling of cultured RPE cells

Fixed cells on coverslips were, sequentially, permeabilised in phosphate buffered saline (PBS; 137 mM NaCl, 5.4 mM KCl, 1.28 mM $NaH_2PO_4$, 7 mM $Na_2HPO_4$; pH 7.4) con-
taining 0.1% (v/v) Triton X-100 (PBS-T) for 15 minutes, further washed in PBS and then blocked in horse serum (3.3%, v/v in PBS; PBS-HS). Antibodies used for cell label- ling (Table 1) were diluted as appropriate in PBS-HS and applied to individual coverslips overnight at room temper- ature. Detection of labels is described in detail in the Supporting Information and was as described previously.[33] Labelled cells were examined with epifluorescence micros- copy (Olympus Australia Pty Ltd, Edwardstown, South Australia). Photography was undertaken with a DP73 camera attachment (Olympus Australia Pty Ltd).

## 2.5 | Quantification of immunocytochemical labelling

Quantification of immunolabelling for cultured RPE cells was performed in one of two ways. The first was applied to antibodies where labelling was clearly confined within discrete and discernible individual cells (cyclin D1, vimentin, nestin): five of the total of 16 individual lased locations were selected from each coverslip and the cen- tre of the treatment area centred in the view field. All cells displaying obvious labelling for the requisite anti- body in the field were scored and counts averaged for the five selected areas. This mean value then became a single determination (n); single coverslips treated from 6 differ- ent cultures, each of which was derived from a separate primary culture, and immunolabelled at different times were thus used to produce 6 individual determinations (n = 6). The second quantification method was applied to antibodies which either labelled large numbers of over- lapping cells (e.g., α-tubulin) or which could not distin- guish cellular boundaries (e.g., Hsp27): here, Image J was
used to quantify "labelling area" per field for the requisite
antibody and then, as before, this value averaged from
5 lased regions per coverslip for 6 separate coverslips (n = 6). In the case of the Hsp27 labelling quantification, data were expressed relative to that obtained for α-tubulin to account for the changing number of cells present within the quantified image.

Comparison of values obtained at each time-point for each labelling experiment at each laser energy versus sham, untreated controls, was carried out by one-way Analysis of Variance (ANOVA) followed by Dunnett's multiple comparison test. In some specific cases, in order to determine whether effects of the laser were different at two or more laser settings, comparison was made between the means of all groups by undertaking a one-way ANOVA followed by Tukey's multiple comparison test.

## 2.6 | Animals

This study was approved by the SA Pathology/Central Heath Network Animal Ethics Committee (Adelaide, Australia) and conformed with the Australian Code of Practice for the Care and Use of Animals for Scientific Purposes, 2013, and with the ARVO Statement for the use of animals in vision and ophthalmic research. Adult Dark Agouti rats (Aged 6-8 weeks; approximately 150 g each) were housed in a temperature- and humidity- controlled room with a 12-h light, 12-h

dark cycle and were provided with food and water ad libitum.

Description of animal treatments is detailed in Supporting Information. Animals were treated in both eyes on a custom-designed platform mounted on a slit- lamp delivery system (Figure 1(G)). Either sham treat-ment was applied ("untreated control" at each time point
for comparative purposes) or actual laser treatment was applied at one of two energy settings (145, 91 mJ/cm$^2$). Typically, 15-20 laser spots were applied through the

TABLE 1    Antibodies used in the study

| Name | #Cat No. *Clone | Host | Company | Dilution ICC | Dilution IHC | Dilution WB |
|---|---|---|---|---|---|---|
| β-Actin | #A5441 | Mouse | Sigma-Aldrich | — | — | 1:10000 |
| αB-crystallin | *G2JF | Mouse | Leica | — | 1:500 | 1:2000 |
| Cyclin-D1 | #AB21699 | Rabbit | Abcam | 1:20 | 1:5 | — |
| Hsp27 | #SPA-801 | Rabbit | Stressgen | 1:2000 | 1:500 | 1:2000 |
| Nestin | *Rat 401 | Mouse | BD Transduction | 1:1000 | — | 1:1000 |
| RPE65 | *8B11 | Mouse | Santa Cruz | 1:2500 | 1:500 | 1:1000 |
| α-Tubulin | #MU121-UC | Mouse | BioGenex | 1:5000 | — | — |
| Vimentin | *V9 | Mouse | Dako | 1:5000 | 1:250 | — |
| ZO-1 | #61-7300 | Rabbit | Invitrogen | 1:1000 | 1:250 | — |

*Note:* Addresses: Sigma-Aldrich, Castle Hill, NSW, Australia; Leica, North Ryde, NSW, Australia; Abcam, Cambridge, UK; Stressgen, Victoria, BC, Canada; BD Transduction Labs, Lexington, KY, USA; Santa Cruz Biotechnology, Santa Cruz, CA, USA; BioGenex, Fremont, CA, USA; Dako, Sydney, NSW, Australia; Invitrogen, Mulgrave, Victoria, Australia.
Abbreviations: ICC, immunocytochemistry on cell cultures; IHC, immunohistochemistry on RPE-choroid wholemounts; WB, Western blotting. Note: IHC was conducted as a 2-step protocol and ICC as a 3-step protocol (see Materials and Methods).

cornea and onto the retina for each eye. Treatment avoided overlapping spots, the optic nerve head region or any major blood vessels (Figure 1(H)). Treated animals were killed at the following times: 0 h (immediately after laser treatment), 6 h, 24 h, 72 h and 7 days. Eight animals were treated per laser setting for each time-point.

## 2.7 | Preparation and labelling of RPE- choroid wholemounts

Animals were perfused with sterilised, physiological saline (0.9%, w/v) followed by NBF, under terminal anaesthesia. Both eyes were enucleated and retinal wholemounts pre- pared and labelled via immunohistochemistry as described in the Supporting Information section. Primary antibodies used (αB-crystallin, cyclin-D1, Hsp27, RPE65, vimentin, ZO-1) are detailed see Table 1). Immunohistochemical labelling is also described in detail in the Supporting Infor- mation section. Data from 4 separate eyes per time point were collected for statistical comparisons (n = 4). Since immunohistochemistry was being used to determine ele- vations in specific antigen expression versus background, data were compared for different time-points against that obtained from time zero; one-way ANOVA followed by post-hoc Dunnett's testing was employed for significance comparisons.

## 2.8 | Scanning electron microscopy (SEM)

Eyes for SEM were enucleated from terminally anaesthetised animals after transcardial perfusion with physiological saline (0.9% w/v) alone. Eye-cups of RPE- choroid were prepared as described above except that tis- sue remained non-fixed at this stage. After dissection into wholemounts, tissues were immersed into 3 mL of elec- tron microscopy fixative (4% w/v, paraformaldehyde plus 1.25% w/v glutaraldehyde and 4% w/v sucrose, pH 7.2, in

PBS) at 4°C for 1 h. Subsequent to this, wholemounts were washed in 4% w/v sucrose in PBS for 5 minutes and then post-fixed in 2% w/v osmium tetroxide in PBS for 1 h at room temperature. Progressive dehydration was then carried out via sequential 15 minute washes in 70% v/v ethanol (x2), 90% v/v ethanol (x2) and absolute etha- nol (x3). In the final immersion in absolute ethanol, eye- cups underwent critical point drying in a Tousimis Super- citical 931.GL Autosamdri (Tousimis, Rockville, MD). Tissue was then mounted on metal stubs and carbon coated. Morphological imaging of treated and non-treated RPE-choroid wholemounts was conducted using a Philips XL40 ESEM Environmental Scanning Microscope (Philips, Eindhoven, Netherlands).

## 2.9 | Electrophoresis and western blotting

Eye-cups of RPE-choroid were prepared as described for SEM and then immersed in 2 mL PBS. A round-head syn- thetic nylon filament artists' paintbrush (size 2) was used to brush RPE cells from Bruch's membrane into the immersing PBS. RPE cells were collected by centrifuga- tion, and cellular extracts prepared and electrophoresis and Western immunoblotting performed as detailed in the Supporting Information section and as described pre- viously.[33] Protein concentrations were equalised in

samples by undertaking a bicinchoninic acid assay, as per manufacturer's instructions (Sigma-Aldrich). Label- ling on blots was quantified (see Supporting Information section) and normalised for levels of β-actin. Samples were prepared from treated animals after 0, 6 and 24 h and data were compared using one-way ANOVA followed by Tukey's multiple comparisons test for signifi- cance, with n = 4 samples per determination.

## 3 | RESULTS

### 3.1 | Effect of laser treatment on cultured RPE cells

Cultured rat RPE cells formed a homogeneous monolayer and retained pigment at the time of treatment (Figure 1 (B)). The cells labelled positively for RPE65 (Figure 1(C)) and ZO-1 (Figure 1(D)), both of which are strongly expressed by RPE cells in vivo. They also labelled for the structural protein α-tubulin (Figure 1(E)), which was employed to assess the effects of laser treatment as it labelled the cells cleanly and homogeneously (Figure 1(F)); this image corresponded to the appearance of the RPE cells prior to laser treatment. Application of 2RT laser to confluent RPE cells at first passage

resulted in

clear and energy-level-dependent effects (Figure 2(A–N)).

A denuded region was induced in the RPE cell layer with immediate effect with the laser energy set above 64 mJ/cm$^2$; at 24 mJ/cm$^2$, there was no observable lesion in the RPE monolayer. The lesions directly produced at the settings of 64, 91 and 145 mJ/cm$^2$ were all of signifi- cant size as compared with control, non-treated cells ($p < 0.001$ by one-way ANOVA followed by Dunnett's multiple comparison test Figure 2(O)) and not signifi- cantly different from each other.

The laser-induced RPE lesions all decreased in size over time and were re-populated with cells by 3–7 days (Figure 2 (J, K, L, P)). At 64 and 91 mJ/cm$^2$, lesions were diminished in size compared with their initial denuded zones by 6 h post-treatment, and by 24 h, even the lesion induced by 145 mJ/cm$^2$ had a significantly smaller diameter. By 72 h after treatment, the remaining denudation produced by the laser at 145 mJ/cm$^2$ but not at any of the lower energy set- tings, was still significantly elevated in size when compared with untreated cells; after 7 days no lesions remained signif- icantly appreciable after any laser application.

## 3.2  |  Expression of Hsp27

After laser treatment, cultured RPE cells close, or adja- cent, to the lesion site expressed Hsp27 by 6 h (Figure 3(A–J)). Where induced, labelling partially co- localised with α-tubulin, indicating that it was predomi- nantly based within the cytoplasm. Although expression of Hsp27 was qualitatively detectable at 6 h post- treatment with all laser settings (Figure 3(A–C)), only when the energy was applied at 91 or 145 mJ/cm$^2$ was the level significantly increased above the background, non-treated level (Figure 3(K)). Expression of Hsp27 remained elevated for 72 h after applying the laser at both 91 and 145 mJ/cm$^2$ (Figure 3). When comparing the relative abundance of Hsp27 expression induced by the 91 and 145 mJ/cm$^2$ power settings, the lower energy level had a somewhat greater effect at 6 h, 24 h and 72 h, although the difference was only significant at 72 h ($p < 0.01$). It is noteworthy that the majority of the cells labelling for Hsp27 after 72 h at the setting of 91 mJ/cm$^2$ were within the re-populated region where a lesion had healed. Also of interest is the finding that the maximum level of induced Hsp27 expression was at 6 h for each setting (Figure 3(K)). There were no cells labelled for Hsp27 after more than 3 days (data not shown).

## 3.3  |  Cyclin D1 expression

Relative to untreated cells (Figure 4(J)), Cyclin D1 expression was rapidly induced in cultured RPE after 2RT laser treatment (Figure 4(A–J)). By 6 h after treat- ment with 145 mJ/cm$^2$, a significant number of cells sur- rounding the denuded region expressed cyclin D1 in their nucleus ($20.3 \pm 1.7$ cells per field versus $0.7 \pm 0.5$ in an equivalent sized area in control cells; $p < 0.001$; Figure 4 (K)). Cyclin D1 remained significantly elevated until 72 h, after which it decreased (Figure 4). At 91 mJ/cm$^2$, expression of cyclin D1 was also significantly increased above background levels after 6–72 h (Figure 4). At 64 mJ/cm$^2$, a significant induction of Cyclin D1 was only apparent after 6 h. All cells, regardless of laser setting applied, had returned to background cyclin D1 expression levels by 7 days post-treatment (Figure 4(K)). No significant labelling for cyclin D1 was detected after 7 days; appearance of labelled cells was similar to untreated cells (Figure 4(J)); although a few sporadic nuclei were still positively labelled after treatment with the laser at 145 mJ/cm$^2$ (Figure 4(L)).

FIGURE 2  Appearance of cultured RPE cells after treatment with 2RT laser. All cells shown have been immunocytochemically labelled with the cytoskeletal protein, α-tubulin, and counter-stained with the nuclear label, DAPI. Culture appearance and density as a result of treatment with laser set at an energy level of (A, D, G, J) 145 mJ/cm$^2$, (B, E, H, K) 91 mJ/cm$^2$ and (C, F, I, L) 64 mJ/cm$^2$. Arrows denote centre of lased zones in each case. (A–C) Cells fixed immediately after treatment, to show lesion appearance in RPE cell monolayer directly as a result of laser treatment. (D–F) Cells fixed 6 h, 24 h (G–I) and 72 h (J–L) after treatment, to show how lesion size and appearance changed over time. (M) Demonstrates how reduction of the laser energy level further (24 mJ/cm$^2$) does not cause any visible lesion in RPE cell layer. (N) Magnified image of cells abutting the periphery of a laser-induced lesion (145 mJ/cm$^2$) at 6 h post-treatment showing cells present within the laser-treated region. (O) Graph showing the relationship between the size of the initial laser lesion and the applied energy level: ***$p < 0.001$ when comparing size of initial laser lesion at each setting versus untreated control, by one-way ANOVA followed by Dunnett's multiple comparison test ($n = 8$). (P) Graph showing how the size of the laser lesion decreases over time, with each of the energy settings applied. ***$p < 0.001$, **$p < 0.01$ when comparing size of lesion versus control cells, by one-way ANOVA followed by Tukey's comparison test ($n = 16$ values per determination). Scale bars: (A–M) = 100 μm; (N) = 100 μm
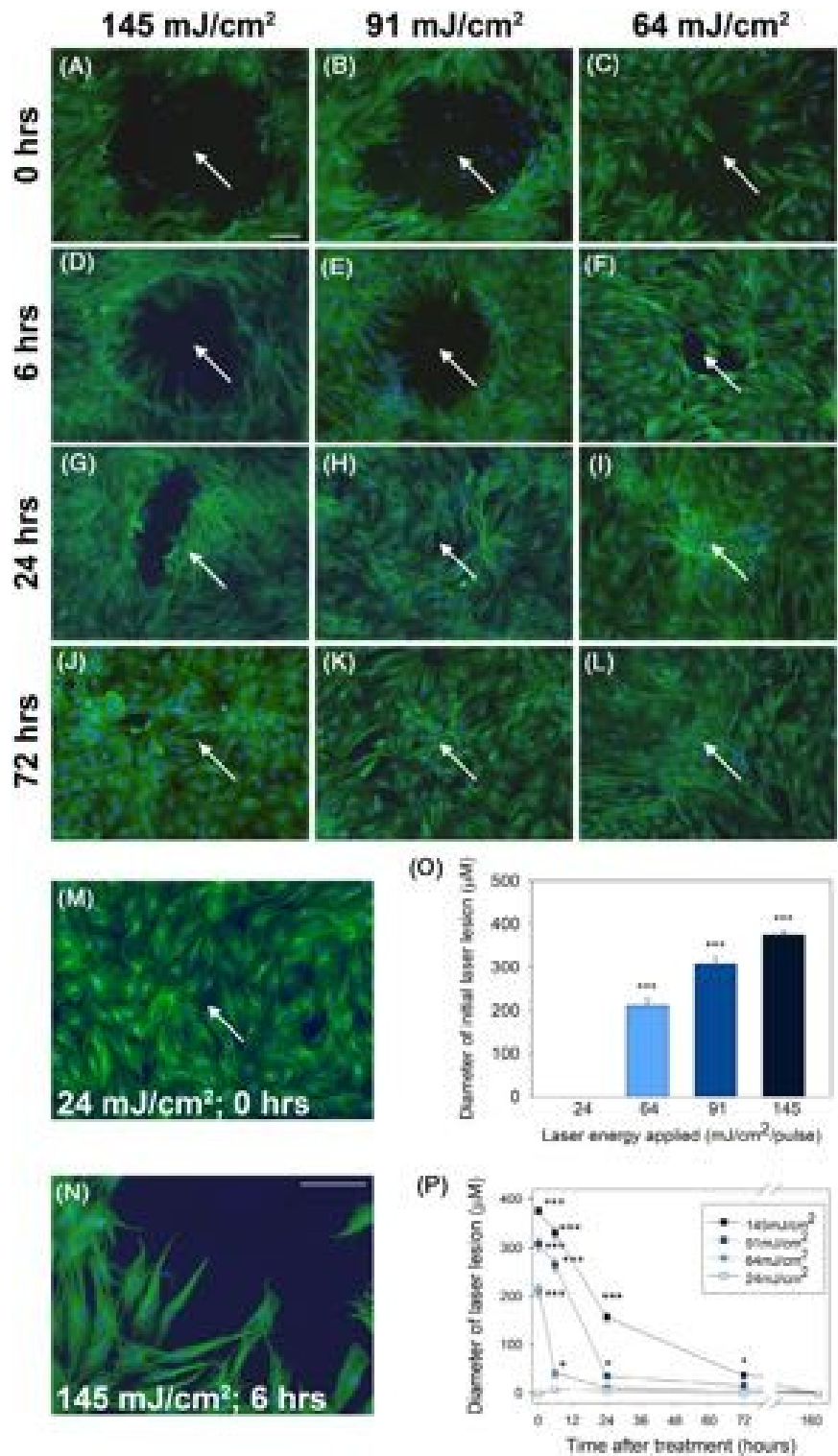


## 3.1 | Intermediate filament proteins

After 2RT laser treatment of cultured RPE cells, cytoplas- mic expression of the intermediate filament protein vimentin was observed, which was not present in un-

treated cells. When present, vimentin expression was always localised either to cells in the treated zone or to cells at the margins of this region. At 24 mJ/cm$^2$, vimentin was only significantly increased after 6 h, whereas at 64 mJ/cm$^2$ and at 91 mJ/cm$^2$ this protein was significantly elevated at both 6 and 24 h although not by 72 h. However, at 145 mJ/cm$^2$, vimentin expression was significantly elevated above background after 6 h and up to 7 days (Figure 5).
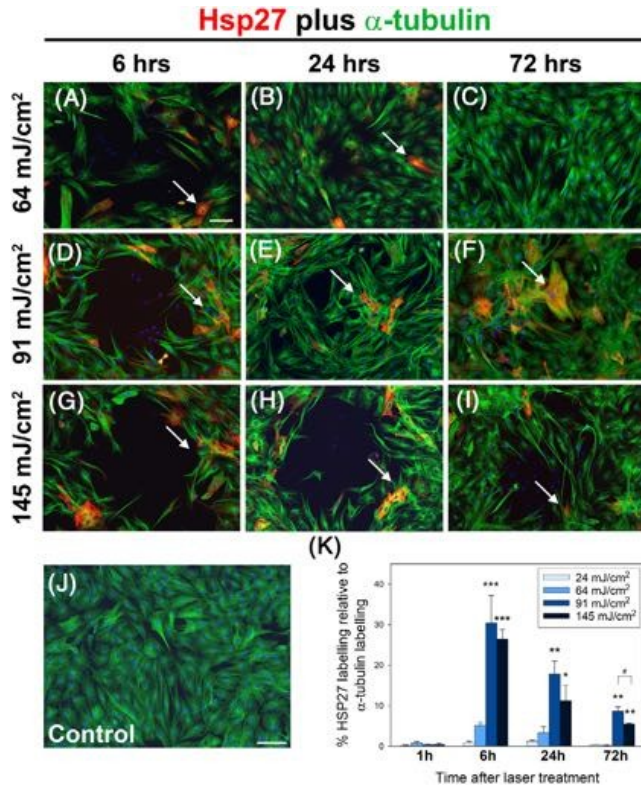
**FIGURE 3** Induction of heat shock protein 27 (Hsp27) expression after treatment of cultured RPE cells with 2RT laser at energy settings of 64 mJ/cm$^2$ (A, D, G), 91 mJ/cm$^2$ (B, E, H),

145 mJ/cm$^2$ (C, F, I); control, untreated cells are also shown (J). All cells shown have been labelled for α-tubulin (green), and Hsp27 (red), and counter-stained with the nuclear label, DAPI (blue).

Cells expressing Hsp27, where labelling co-localises with α-tubulin, appear yellow. Cells were analysed at 6 h (A–C), 24 h (D–F), and 72 h (G–I). (K) Quantification of labelling for Hsp27. ***$p < 0.001$,

**$p < 0.01$, *$p < 0.05$, when comparing data obtained at each energy setting versus untreated control values, for each time-point, by one-way ANOVA followed by Dunnett's multiple comparison test ($n = 3–6$ values per determination). Scale bar: 100 μm

The intermediate filament protein, nestin was induced in a similar manner to vimentin. Nestin was not present in untreated cells, but laser application to cultured RPE cells led to expression of nestin in cells immediately surrounding the treated zone or in repopulating cells within this region after 6 h or more (Figure 5(M–R,T)). At 64 mJ/cm$^2$, expression of nestin was significantly elevated only after 6 h (Figure 5(T)), at 91 mJ/cm$^2$ after 6, 24 and 72 h with a maximum induc- tion at 24 h (Figure 5(M–O,T)), and at 145 mJ/cm$^2$ after

6, 24, 72 h and 7 days with the maximum stimulation after 72 h (Figure 5(P–R,T)). Use of the laser at 24 mJ/cm$^2$ did not lead to any significant induction of nestin expression.

## 3.2 | Tight junctions

In culture, rat RPE cells express Zonula occludens-1 (ZO-1) at their cellular boundaries, indicating the existence of
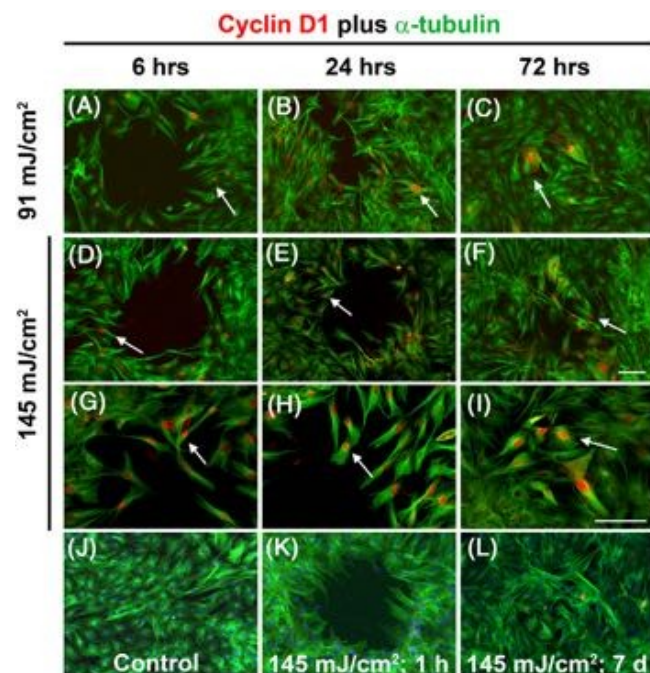
FIGURE 4    Induction of cyclin D1 expression in cultured RPE cells subjected to 2RT laser at energy settings of 91 mJ/cm$^2$ (A–C) and 145 mJ/cm$^2$ (D–I, K, L); control, untreated cells are also shown (J). All cells shown have been labelled for α-tubulin (green) and cyclin D1 (red), and counter-stained with the nuclear label, DAPI (blue). Cells were fixed at 6 h (A, D, G), 24 h (B, E, H) or 72 h (C, F, I). Images shown in (G–I) represent higher magnification images of cells treated as in (D–F). Labelling at 1 h (K) and 7 days (L) is also shown for 145 mJ/cm$^2$. (M) Quantification of cyclin D1 expression. ***$p < 0.001$, **$p < 0.01$, *$p < 0.05$, when comparing data obtained at each energy setting versus untreated control values, for each time-point, by one-way ANOVA followed by Dunnett's multiple comparison test ($n = 6$ values per determination). Scale bars are all 100 μm: Scale bar shown in (F) corresponds to the scale of images (A–F, J–L); scale bar shown in (I) refers to the magnification shown in (G–I)

tight junction machinery (Figure 6(A)). At 6 h after treat- ment with the 2RT laser, there was an ablation of RPE cells with the corresponding loss of ZO-1 protein (Figure 6(B)). At this stage, cells outside of the treated region still retained some ZO-1 (Figure 6(B)). As the cells re-populated the lesion site and came into contact with one another, there was a renewed expression of ZO-1, although it was somewhat disorganised (Figure 6(C)).
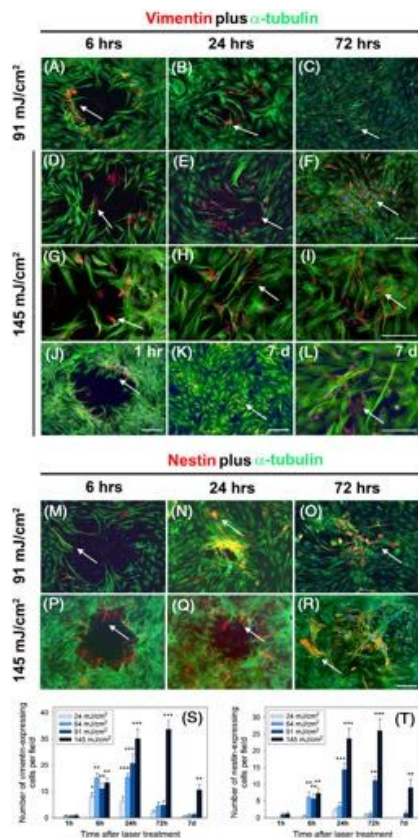
**FIGURE 5** Induction of expression of the intermediate filament proteins, vimentin (A–I, M) and nestin (J–L, N), in cultured RPE cells after treatment with 2RT laser. (A–I) Cells shown have been labelled for α-tubulin (green), and vimentin (red; arrows) and counter-stained with the nuclear label, DAPI (blue). Cells were treated with laser setting at 91 mJ/cm$^2$ (A–C) and 145 mJ/cm$^2$ (D–L) and fixed after 1 h (J), 6 h (A, D, G), 24 h (B, E, H), 72 h (C, F, I) or 7 days (K, L). Images shown in (G–I, L) represent higher magnification images of cells treated as in (D–F, K), respectively. (P) Quantification of vimentin expression by 2RT laser at different energy settings and times post-treatment. (M–R) Cells treated with laser at 91 mJ/cm$^2$ (M–O) or 145 mJ/cm$^2$ (P–R), fixed after 6 h (M, P), 24 h (N, Q) or 72 h (O, R) and then labelled for α-tubulin (green), and nestin (red; arrows) and counter-stained with the nuclear label, DAPI (blue). (Q) Quantification of nestin expression. ***$p < 0.001$, **$p < 0.01$, *$p < 0.05$, when comparing data obtained at each energy setting versus untreated control values, for each time-point, by one-way ANOVA followed by Dunnett's multiple comparison test ($n = 6$ values per determination). Scale bars are all 100 μm: scale bar shown in (F) relates to magnification shown in (A–F); scale bar shown in (I) is representative of the magnification used for (G–I); scale bars shown in (J–L) relate to the single images in which they are based; scale bar shown in (R) relates to the magnification shown in images (M–R)

After 7 days, when the lesion site had completely healed, the cells in this location had regained a normal pattern of ZO-1 expression (Figure 6(D)).

## 3.3 | Effect of 2RT laser on RPE cells in vivo

RPE cells analysed in wholemount preparations had a homogeneous appearance, but were clearly multi- nucleate (Figure 1(I)).

Two energy settings were tested for the 2RT laser in vivo: 91 and 145 mJ/cm$^2$. Scanning electron micros- copy (SEM) imaging of wholemounts prepared immedi- ately after laser treatment at 91 mJ/cm$^2$ and 145 mJ/cm$^2$, revealed the denuded region of the RPE monolayer and underlying Bruch's membrane (Figure 7(A,E), respec- tively). After 24 and 72 h, cells had reappeared in the denuded zone (Figure 7(B,F) and (C,G), respectively). Higher power electron microscopy revealed that after 7 days cells had replenished the ablated region. Imaging revealed that the RPE cell layer was once again intact (Figure 7(D,H)).

Labelling for ZO-1 in untreated eyes revealed cell perimeters and allowed dissemination of RPE cells in relation to the laser lesion site (Figure 7(M)). When laser was applied at the visible effect threshold of 145 mJ/cm$^2$, a region was observed in which ZO-1 labelling was absent and Bruch's membrane was revealed. The lesion was still clearly visible at 1, 3 and 7 days post-treatment, indicating that at this energy level there was incomplete

functional repair of the RPE monolayer in this time- frame (Figure 7(N–P)). However, between 3 and 7 days after lasing, irregularly-shaped cells re-populated the edges of this region as demonstrated by the reappearance of ZO-1 (Figure 7(P)). After application of laser at the lower setting of 91 mJ/cm$^2$ there was a similar pattern of labelling up to 3 days (Figure 7(I–K)). However, the lesion was repaired by 7 days post-treatment (Figure 7(L)).

The RPE-specific protein, RPE65, was clearly and dis- tinctly labelled in cells in wholemounts from both untreated (Figure 1(I)) and treated (Figure 7(Q–W)) ani- mals. Application of laser at either 91 mJ/cm$^2$ (Figure 7(Q–T)) or 145 mJ/cm$^2$ (Figure 7(U–W)) caused visible lesions that could be quantified (Figure 7(X)). In the case of the higher setting of the laser, there was a slow, partial replenishment of RPE cells into the denuded region, which was visible by 3 days (Figure 7(V)) and more fulsome by 7 days (Figure 7(W,X)). Nevertheless,

the lesion was still only partially healed at this time (Figure 7(W,X)). In contrast, treatment at 91 mJ/cm$^2$ cau- sed a lesion that was partially replete with cells by 24 h (Figure 7(R,X)), had much of the denuded zone replenished by 3 days (Figure 7(S,X)) and, remarkably, was almost completely healed by 7 days (Figure 7(T,X)). The application of laser was found to be consistent between individual eyes since quantification of lesion
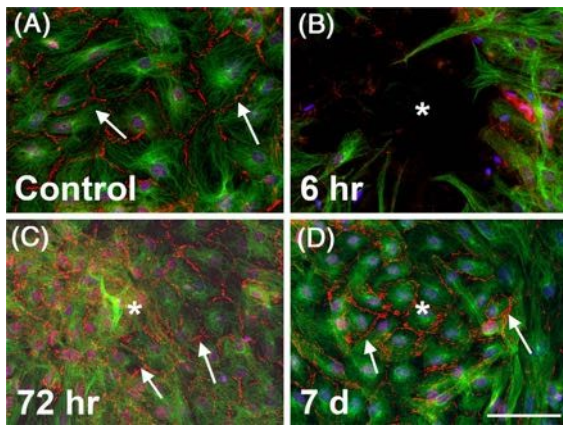
**FIGURE 6** Immunocytochemical localisation of the tight junction protein, ZO-1, in cultured rat RPE cells and the effect of 2RT laser treatment. Cells shown have been labelled with α-tubulin (green), and ZO-1 (red; arrows) and counter-stained with DAPI (blue). (A) Control, untreated cells showing clear labelling for ZO-1 at intercellular boundaries. (B) Cells shown 6 h after treatment with 2RT laser applied at 91 mJ/cm$^2$; laser-induced lesion site indicated by *. (C) At 72 h after laser exposure, cells have re- populated the lesion area and expression of ZO-1 is present but arranged in a disorganised manner. (D) After 7 days, cells at lesion site have regained a normal expression pattern of ZO-1. Data are shown only for the 91 mJ/cm$^2$ setting for illustrative purposes.
Scale bar: 100 μm

sizes at each time-point showed relatively limited vari- ability (Figure 7(X)).

## 3.4 | Wound-healing response in vivo

Induction of proteins involved in wound-healing and remodelling of the RPE was investigated only with use of the laser at the setting used in the clinical trials, 91 mJ/cm$^2$, for the sake of clarity. Firstly, cell prolifera- tion as identified by immunolabelling with cyclin D1 was detected by 6 h post-treatment (Figure 8(B)). Quantifica- tion of labelling within 200 μm of the centre of the lased area revealed a maximum labelling after 6 h. Numbers of cells were significantly increased above control at 6 h post-treatment (Figure 8(B,C)).

Vimentin was not present in wholemounts from untreated animals but was clearly induced at 24 and 72 h after laser application, in cells at the edges of the lased regions (Figure 8(D,E)). Quantification of vimentin- labelled cells within 200 μm of the irradiated region delineated that there was a significant increase up to 72 h after treatment, after which there was a rapid decline.

The small heat shock protein family member, αB- crystallin, was not detected in untreated samples, but was rapidly and significantly induced in RPE cells in the peri-

treated region (Figure 8(G–K)). This was clear at 6 h and was more prominent after 24 h, also revealing that cells had become elongated and were in the process of popu- lating the denuded region. By 72 h labelling had decreased and was only associated with a small number of cells at the centre of the treated site. By 7 days post- treatment there were no longer any cells labelling for this protein.

The 2RT laser also stimulated expression of Hsp27 (Figure 8(L–N)), which was not present in untreated samples. Hsp27 Western immunoblotting revealed that there were significant and detectable increases at 6 and 24 h. Immunohistochemical labelling also revealed that
some RPE cells at the centre of the treated region remained positive for Hsp27 expression after 72 h.

## 4 | DISCUSSION

In the present study we undertook a detailed investiga- tion into the wound-healing response of the RPE to 2RT laser treatment, since this process likely underlies the beneficial effect of the laser on dry AMD progres- sion.[27,30,31] In agreement with previous studies,[19,21,29,30] our data clearly show that the 2RT laser caused an energy-dependent and selective ablation of RPE cells in vitro and in vivo, which was likely predominantly via vaporisation, as evidenced by the lack of cell material within lesion sites immediately after treatment. Our data also clearly show that the RPE layer was subsequently replenished. Rapid RPE layer re-epithelialisation after injury and consequent barrier re-establishment is well- described,[13,34] including after laser-induced damage.[35,36] This process is crucial because if it did not occur, then RPE-depletion itself would indirectly damage adjacent photoreceptors, therefore negating the use of this form of therapy.

What are the actual cellular triggers that stimulate surviving RPE cells to initiate re-epithelialisation? Sug- gestions have included physical damage to cells at the insult boundary with the consequent release of cellular constituents, the sudden availability of permissive, non- contact-inhibited cell boundaries, and the non- physiological exposure of basement membrane.[37] For example, the loss of cell-cell contacts after wounding of the RPE cell layer has been found to act as a strong stim- ulus for the process of re-epithelialisation.[38] It is also likely that sub-lethal stress to adjacent cells during a trau- matic incident activates healing mechanisms.[37] In the present study, we detected the rapid elevation of expres- sion of Hsp27 and αB-crystallin in cells bordering lesion sites. These proteins are both members of the small heat shock protein family and can be induced by processes

**FIGURE 7** Assessment of the effects of 2RT laser application on RPE in vivo. Laser was applied to an eye of a live animal and RPE wholemounts prepared. (A–H) Scanning electron microscopy of region treated by laser at 91 mJ/cm$^2$ (A–D) and 145 mJ/cm$^2$ (E–H), indicating lesion in RPE monolayer (shown by red asterisks) and revealing underlying Bruch's membrane (BM). Times after treatment are recorded ((A, E): 0 h; (B, F): 24 h; (C, G): 3 days; (D, H): 7 days) and arrows indicate where RPE cells have re-populated lesion site; during re-populations, some cells within the lesion site are flattened and lack apical microvilli (C, arrowhead). Scale bars are as follows: (A, E): 50 μm; (B, F): 40 μm; (C, G): 20 μm; (D, H): 10 μm. Immunohistochemical labelling of RPE wholemounts for the tight junction protein, ZO-1 (I–P) and the RPE-specific protein, RPE65 (Q–W), at indicated laser energy settings and times after treatment. Red asterisks indicate lesion sites and arrows indicate RPE cell reappearance. When applied at 91 mJ/cm$^2$, the lesion site was rapidly filled by re-populating cells (I–L, Q–T): by 7 days post-treatment the RPE monolayer has effectively been completely regenerated (L, T). Although some replenishment of killed cells occurs at 145 mJ/cm$^2$ a visible lesion still existed after 7 days (P, W). (P) Quantification of post-treatment lesion size diameter verified these findings. Scale bar (shown in (P)): (I–W) = 50 μm
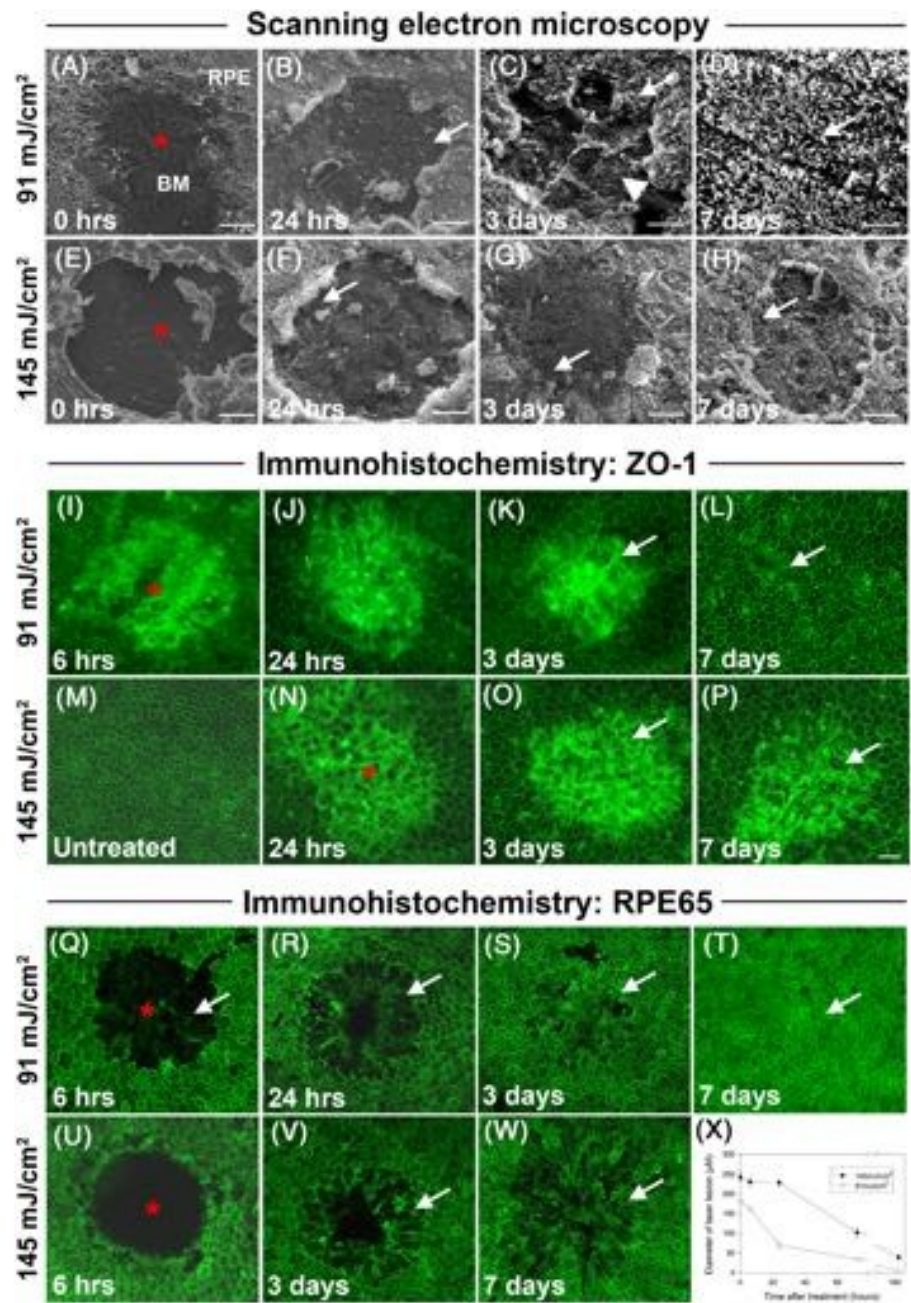


such as thermal increases or oxidative stress occurring at the edge of the lesion.[39] Induction of small heat shock pro- teins is likely to assist in both chaperone-mediated protec- tion of proteins and contribute to ongoing repair of the epithelial layer, particularly by virtue of their ability to reg- ulate cytoskeletal actin dynamics[40] and the inhibition of apoptosis.[41] Hsp27 induction has been demonstrated previ- ously in RPE cells in response to different stresses.[42] αB- crystallin is expressed in the RPE during development, and, as a result of retinopathy.[43] This protein is also expressed in damaged RPE and Bruch's membrane in dry AMD.[44,45] αB-crystallin is believed to promote protection of RPE cells from a range of stressors.[43]

The expression of small heat shock proteins such as Hsp27 and αB-crystallin also promotes epithelial- mesenchymal transition (EMT),[46,47] an epithelial de- differentiation involving the loss of cell polarity and intercellular adhesion, and the gain of migratory poten- tial.[37] Quiescent layered cells generally undertake this process to repair lesions, before reversion to their original states via a reverse process (mesenchymal epithelial tran- sition; MET). EMT is controlled by the activation of transcription factors, such as Snail 1 and Snail 2, by sig- nalling pathways such as those mediated by transforming growth factor β (TGF-β), bone morphogenetic protein (BMP), or epidermal growth factor (EGF).[48] Such
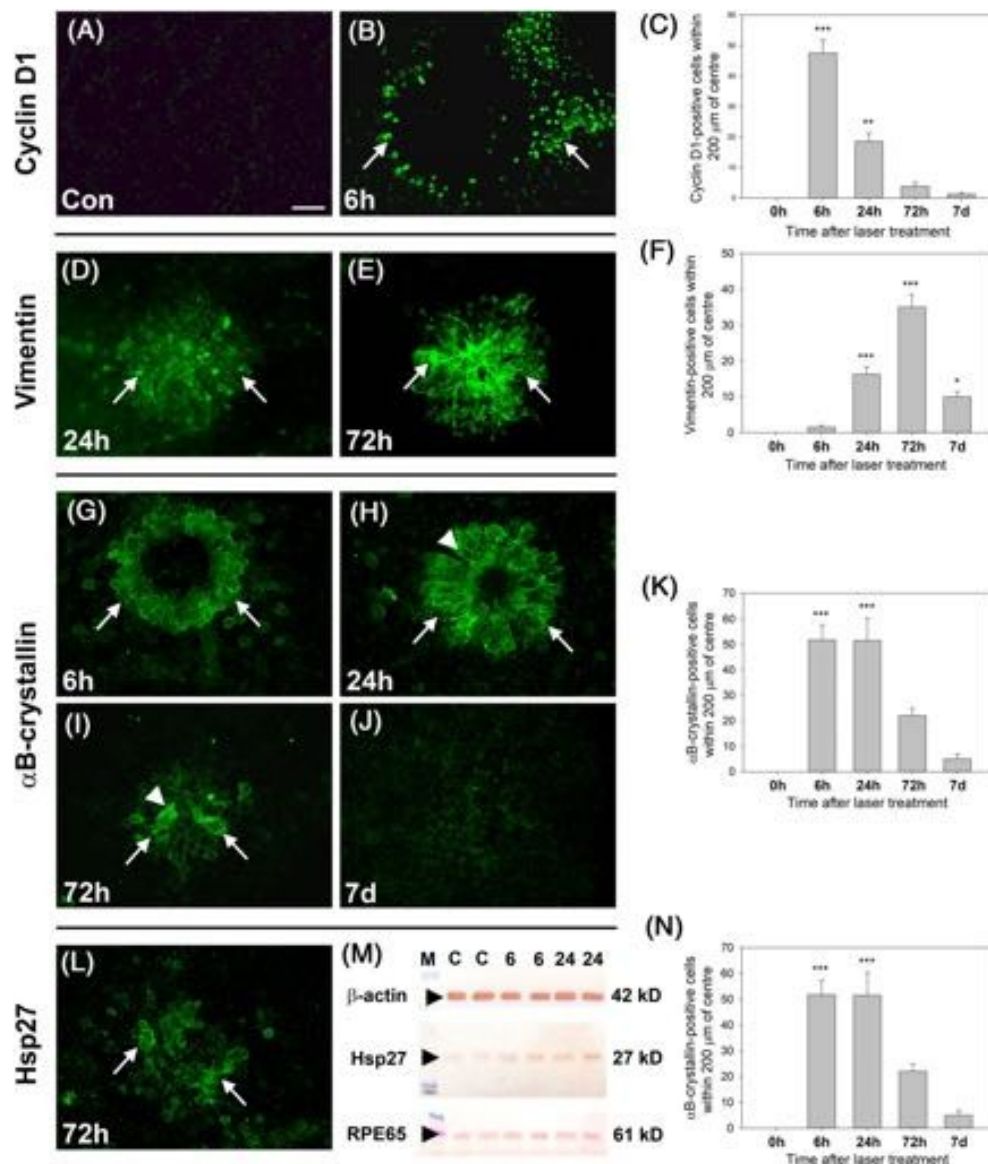
**FIGURE 8** Stimulation of protein expression in RPE cells exposed to 2RT laser (91 mJ/cm$^2$) in vivo, in RPE wholemounts. (A–C) Cyclin D1 expression is induced by laser irradiation (B; 6 h post treatment) in the nuclei of cells at the periphery of the lesion site, as compared with untreated cells (A). Quantification of cyclin D1 induction over time, post treatment is shown in (C). (D–F) Induction of vimentin expression. Labelling is observed in some cells after 24 h (D), but expression is more pronounced after 72 h (E). Quantification of vimentin induction over time (F). (G–K) Induction of αB-crystallin expression. Within 6 h, there is a clear expression of αB-crystallin (G; arrows). Over time, these cells repopulate the treated region (H, I) until, by 7 days post-treatment, the lesion has been repaired and expression of αB-crystallin has diminished to background levels (J). Quantification of αB-crystallin induction over time (K). (L–N) Induction of Hsp27 labelling in lased cells. Hsp27 expression is observed in repopulating cells after 72 h (L); Western blot analysis determined increases in Hsp27 expression; "C", control, $t = 0$ treated sample, "6" and "24" refer to the time post-laser treatment (M, N). ***$p < 0.001$, **$p < 0.01$, *$p < 0.05$, when comparing data obtained at each energy setting versus untreated control values by one-way ANOVA followed by Dunnett's multiple comparison test ($n = 4$ values per determination; $n = 4$ separate samples for Western blot). Scale bar: (A, B, D, E, G–J, L) = 50 μm

aberrant signalling will alter transcription of E-cadherin, the pivotal event stimulating EMT.[48] In the present study, activation of small heat shock proteins in cells bordering the lased region is likely to act as one of the initiating events for EMT. Pertinent to this, over-expression of αB- crystallin promotes EMT and additionally, suppression of this protein inhibits EMT in the RPE in vivo.[49]

Interestingly, several other studies have shown induc- tion of the large heat shock protein, Hsp70, after thermal laser application to the RPE.[50,51] Elegant studies by Palanker and colleagues, for example, have demonstrated that photo-thermal treatment of rat eyes induces Hsp70 formation in RPE cells even when targeted at sub-lethal energy levels.[51,52] Recent reports have suggested that

along with selective RPE targeting, sub-lethal laser treat- ment of RPE can also produce a positive therapeutic out- come for a range of outer retinal diseases such as dry AMD, and it is believed that induced expression of Hsp70 in living cells underlies this protective response.[15] How- ever, there is no clear evidence to support intracellular Hsp70 having a role in EMT induction.

The first stage of EMT induction in epithelial cells is the deconstruction of intercellular junctions to allow sep- aration at cell-cell borders.[37,48] This is illustrated in the present study by the loss of the tight junctional protein, ZO-1, in cells adjacent to the laser lesion site (Figure 6). As a corollary of this, the reverse process, MET, is also illustrated in the present study by the new expression and correct organisation of ZO-1 after the lesion in the RPE layer has been repaired. The second stage of EMT includes the initiation of cell motility, a process that involves the suppression of cytokeratin expression and the induction of expression of the intermediate filament protein, vimentin.[37,48] In the present study, we clearly show induction of vimentin expression within 6 h in vitro, with expression still remaining after 7 days at the highest laser energy applied. Furthermore, vimentin was also significantly expressed in RPE cells in vivo from 1 to 7 days after laser application. These data clearly illus- trate the induction of EMT. Of interest was the additional detection of increased levels of nestin in surviving RPE cells after laser treatment, in vivo. Nestin is also an inter- mediate filament protein and is structurally related to vimentin, but it is generally considered to be expressed during development or by progenitor cells in the nervous system.[53] Nestin expression is also induced in retinal Muller glial cells in response to a wide range of injuries, for example experimental glaucoma,[54] and there is evi- dence that adult human RPE cells can also express this protein in vitro.[55] Some evidence also exists, however, associating nestin expression with EMT,[56,57] although whether this protein plays a key part in the cytoskeletal remodelling associated with this process here, or is just induced as part of a generic stress response is unclear.

RPE cells that transition to mesenchymal-like cells can subsequently undertake a number of processes that contribute to cell layer repair. These cellular processes include migration, proliferation or enlargement.[37,58] In the present study we could not definitively state that RPE migration into the wound site occurred, either in vitro or in vivo, because we did not perform migration assays, but it is possible that cell migration contributed to some extent. In vitro, cells appeared within the lesion site within 6 h of treatment, but all such cells were labelled positively for active cell division, implying that re- epithelialisation also involved some proliferation. Cell proliferation was discerned via positive labelling for

cyclin D1. During the G1 phase of the cell cycle, cyclin D1 is synthesised and accumulates in the nucleus; it is degraded in the S-phase.[59] It therefore acts as an unam- biguous marker of cells undergoing active proliferation. We initially detected cyclin D1 in cells surrounding the irradiated region, both in vitro and in vivo, as early as 6 h post-treatment, and subsequently in cells that were re- populating this area, for up to 72 h. RPE proliferation after injury or trauma has been well-documented[34] and, pertinently, has previously been shown 24 h after 2RT treatment in rat eyes[8] and in cells bordering the treated region in both mouse eyes[30] and human Bruch's membrane-RPE-choroid explants.[7] RPE proliferation has also been demonstrated after SRT laser application[5,60,61] and after standard laser photocoagulation.[62]

RPE cells are post-mitotic in situ and therefore do not divide under normal circumstances.[63] Because of this, it is usually thought that reparation to RPE layer lesions is via cell migration. Cell fusion is also thought to play a role, as evidenced by the presence of large, multinucleate RPE cells in situ.[64] Recent data have proven, however, that RPE cells do have the capacity divide in situ, after a range of localised injuries (see Stern and Temple[65]). Fur- thermore, it has now been suggested that the enlarged, multinucleate RPE cells result from incomplete or failed division rather than fusion of neighbouring cells.[66] We clearly detected cells with the appearance of being stretched or enlarged, during RPE layer repair, as reported previously after 2RT,[29,30] SRT[5,60,61,67] pattern scanning laser[68] or standard laser photocoagulation.[62] Cell enlargement can also form a stage in the process of proliferation: the increase in cellular materials ahead of cell division is necessary to produce functional daugh- ter cells. In the case of the RPE, hypertrophic cells can become a problem if they persist, because they do not form physiological associations with outer segments and, therefore, photoreceptor loss can result. In the present study, however, cell enlargement occurred before full reparation of the RPE and did not persist.

RPE division is certainly uncommon in humans, only occurring when lesions occur in the monolayer and nor- mal cell-to-cell contacts become disturbed.[38] When it does occur, RPE proliferation has been suggested to likely occur via EMT, which produces fibroblast-like cells, themselves contributing to local pathology (see Zhou et al[69]). Our data do show that all of RPE cell prolifera- tion, cell enlargement and multi-nucleation are detected during tissue repair in situ. The RPE cells in our untreated whole-mounts, however, are already predomi- nantly multi-nucleate (Figure 1(I)), so occurrence of this process is unlikely to constitute a specific stage of the wound-healing response. Furthermore, enlarged cells around the periphery of lesions appear within 24 h,

which is the same time as cyclinD1-positive cells appear, indicating that cell stretching is occurring concurrently with cell proliferation. Regardless of the absolute balance between cell migration, enlargement and proliferation to promote lesion repair in our system, however, we have shown that although RPE cells undergo EMT, they do in fact revert to their native state after the lesion is rep- opulated. Furthermore, they undertake this process both in vitro and, importantly, in vivo. Thus, the procession of RPE cells through EMT and MET is not pathological but is central to the reparative process.

In conclusion, the combined data demonstrated that ablation of cells within the RPE layer by application of the 2RT laser stimulated a repair process in remaining cells, which eventually replenished lesion sites via the process of EMT. Since this replenishment is necessarily associated with tissue remodelling, then the selective targeting of the RPE with nanosecond pulse lasers such as the 2RT system described here could serve as a useful tool in the consideration of ocular disease treatment. Clinical trials are already underway with this laser to investigate this premise.[27,30] An important additional con- sideration in the use of thermal lasers to treat AMD is that even though drusen presence may be lowered and visual performance improved, new choroidal neovascularisation (CNV) can be stimulated, particularly at the edge of the laser scar.[70-73] This is thought to arise via localised inflammatory production of pro-angiogenic factors or through direct disruption of Bruch's mem- brane. The 2RT laser neither disrupts Bruch's membrane[19] nor induces a significant inflammatory response,[8,28] in comparison with a standard pho- tocoagulator laser. This provides additional support for the preferential use of this laser system for retinal disease treatment.

Finally, the present study sought to address the direct effects of the 2RT laser on RPE cells, in order to under- stand aspects of the mechanism by which it could poten- tially enhance outer retinal functioning. An obvious limitation of this study, however, is that it was carried out on healthy RPE cells in (pseudo-) physiological con- ditions, that is, non-diseased tissue. It is crucial that a succeeding study should assess the influence that 2RT treatment could have in situations that mimic the rele- vant clinical situation, for example, either AMD, as pres- ented in patients, or in a relevant animal disease model. It is also crucial that future studies address the effects of laser treatment as well as post-laser tissue recovery on both the extracellular matrix and the underlying photore- ceptors. Finally, RPE cells are known to differ in their migratory responses to cues according to age of donor and time in culture (in vitro "maturity" level).[74] It must, therefore, be borne in mind that cells having been either

derived from adult rats or that had been cultured for much longer periods of time than in the present study could show different responses to 2RT.

## CONFLICT OF INTEREST

All authors explicitly state that they have no conflicts of interest in connection with this article. NB. Malcolm Plunkett was formerly an employee of Ellex R&D Pty Ltd, but did not retain this capacity during his involve- ment with this study.

## ORCID

*John P. M. Wood* https://orcid.org/0000-0001-8233- 7640
*Robert J. Casson* https://orcid.org/0000-0003-2822-4076

## REFERENCES

1. Sparrow JR, Hicks D, Hamel CP. The retinal pigment epithe- lium in health and disease. *Curr Mol Med*. 2010;10:802-823.
2. Strauss O. The retinal pigment epithelium in visual function. *Physiol Rev*. 2005;85:845-881.
3. de Jong PT. Age-related macular degeneration. *N Engl J Med*. 2006;355:1474-1485.
4. Dorin G. Evolution of retinal laser therapy: minimum intensity photocoagulation (MIP). Can the laser heal the retina without harming it? *Semin Ophthalmol*. 2004;19:62-68.
5. Richert E, Koinzer S, Tode J, et al. Release of different cell mediators during retinal pigment epithelium regeneration fol- lowing selective retina therapy. *Invest Ophthalmol Vis Sci*. 2018;59:1323-1331.
6. Gallagher-Colombo S, Maminishkis A, Tate S, Grunwald GB, Philp NJ. Modulation of MCT3 expression during wound healing of the retinal pigment epithelium. *Invest Ophthalmol Vis Sci*. 2010;51:5343-5350.
7. Zhang JJ, Sun Y, Hussain AA, Marshall J. Laser-mediated acti- vation of human retinal pigment epithelial cells and concomi- tant release of matrix metalloproteinases. *Invest Ophthalmol Vis Sci*. 2012;53:2928-2937.
8. Chidlow G, Shibeeb O, Plunkett M, Casson RJ, Wood JP. Glial cell and inflammatory responses to retinal laser treatment: comparison of a conventional photocoagulator and a novel, 3-nanosecond pulse laser. *Invest Ophthalmol Vis Sci*. 2013;54: 2319-2332.
9. Chu Y, Humphrey MF, Alder VV, Constable IJ. Immunocyto- chemical localization of basic fibroblast growth factor and glial fibrillary acidic protein after laser photocoagulation in the

Royal College of Surgeons rat. *Aust N Z J Ophthalmol*. 1998;26: 87-96.

10. Farnoodian M, Halbach C, Slinger C, Pattnaik BR, Sorenson CM, Sheibani N. High glucose promotes the migra- tion of retinal pigment epithelial cells through increased oxida- tive stress and PEDF expression. *Am J Physiol Cell Physiol*. 2016;311:C418-C436.

11. Heriot WJ, Machemer R. Pigment epithelial repair. *Graefes Arch Clin Exp Ophthalmol*. 1992;230:91-100.

12. Paulus YM, Jain A, Gariano RF, et al. Healing of retinal photo- coagulation lesions. *Invest Ophthalmol Vis Sci*. 2008;49:5540- 5545.

13. Wang H, Ninomiya Y, Sugino IK, Zarbin MA. Retinal pigment epithelium wound healing in human Bruch's membrane explants. *Invest Ophthalmol Vis Sci*. 2003;44:2199-2210.

14. Pollack A, Korte GE. Repair of retinal pigment epithelium and its relationship with capillary endothelium after krypton laser photocoagulation. *Invest Ophthalmol Vis Sci*. 1990;31:890-898.

15. Chhablani J, Roh YJ, Jobling AI, et al. Restorative retinal laser therapy: present state and future directions. *Surv Ophthalmol*. 2018;63:307-328.

16. Brinkmann R, Huttmann G, Rogener J, Roider J, Birngruber R, Lin CP. Origin of retinal pigment epithelium cell damage by pulsed laser irradiance in the nanosecond to microsecond time regimen. *Lasers Surg Med*. 2000;27:451-464.

17. Marshall J. Thermal and mechanical mechanisms in laser dam- age to the retina. *Invest Ophthalmol*. 1970;9:97-115.

18. Marshall J, Hamilton AM, Bird AC. Histopathology of ruby and argon laser lesions in monkey and human retina. A com- parative study. *Br J Ophthalmol*. 1975;59:610-630.

19. Wood JP, Shibeeb O, Plunkett M, Casson RJ, Chidlow G. Reti- nal damage profiles and neuronal effects of laser treatment: comparison of a conventional photocoagulator and a novel 3-nanosecond pulse laser. *Invest Ophthalmol Vis Sci*. 2013;54: 2305-2318.

20. Roider J, Brinkmann R, Wirbelauer C, Laqua H, Birngruber R. Retinal sparing by selective retinal pigment epithelial photoco- agulation. *Arch Ophthalmol*. 1999;117:1028-1034.

21. Wood JP, Plunkett M, Previn V, Chidlow G, Casson RJ. Nano- second pulse lasers for retinal applications. *Lasers Surg Med*. 2011;43:499-510.

22. Tode J, Richert E, Koinzer S, et al. Selective retina therapy reduces Bruch's membrane thickness and retinal pigment epi- thelium pathology in age-related macular degeneration mouse models. *Transl Vis Sci Technol*. 2019;8:11.

23. Roider J, Liew SH, Klatt C, et al. Selective retina therapy (SRT) for clinically significant diabetic macular edema. *Graefes Arch Clin Exp Ophthalmol*. 2010;248:1263-1272.

24. Roider J, Michaud NA, Flotte TJ, Birngruber R. Response of the retinal pigment epithelium to selective photocoagulation. *Arch Ophthalmol*. 1992;110:1786-1792.

25. Casson RJ, Raymond G, Newland HS, Gilhotra JS, Gray TL. Pilot randomized trial of a nanopulse retinal laser versus conventional photocoagulation for the treatment of diabetic macular oedema. *Clin Experiment Ophthalmol*. 2012;40: 604-610.

26. Pelosini L, Hamilton R, Mohamed M, Hamilton AM, Marshall J. Retina rejuvenation therapy for diabetic macular edema: a pilot study. *Retina*. 2013;33:548-558.

27. Guymer RH, Wu Z, Hodgson LAB, et al. Subthreshold nano- second laser intervention in age-related macular degeneration: the LEAD randomized controlled clinical trial. *Ophthalmology*. 2019;126:829-838.

28. Chidlow G, Plunkett M, Casson RJ, Wood JP. Investigations into localized re-treatment of the retina with a 3-nanosecond laser. *Lasers Surg Med*. 2016;48:602-615.

29. Vessey KA, Ho T, Jobling AI, et al. Nanosecond laser treatment for age-related macular degeneration does not induce focal vision loss or new vessel growth in the retina. *Invest Ophthalmol Vis Sci*. 2018;59:731-745.

30. Jobling AI, Guymer RH, Vessey KA, et al. Nanosecond laser therapy reverses pathologic and molecular changes in age- related macular degeneration without retinal damage. *FASEB J*. 2015;29:696-710.

31. Guymer RH, Brassington KH, Dimitrov P, et al. Nanosecond- laser application in intermediate AMD: 12-month results of fundus appearance and macular function. *Clin Experiment Ophthalmol*. 2014;42:466-479.

32. Mayerson PL, Hall MO, Clark V, Abrams T. An improved method for isolation and culture of rat retinal pigment epithe-     lial cells. *Invest Ophthalmol Vis Sci*. 1985;26:1599-1609.

33. Wood JP, Mammone T, Chidlow G, Greenwell T, Casson RJ. Mitochondrial inhibition in rat retinal cell cultures as a model of metabolic compromise: mechanisms of injury and neuroprotection. *Invest Ophthalmol Vis Sci*. 2012;53:4897-4909.

34. Grierson I, Hiscott P, Hogg P, Robey H, Mazure A, Larkin G. Development, repair and regeneration of the retinal pigment epithelium. *Eye*. 1994;8:255-262.

35. Lammer J, Bolz M, Baumann B, et al. Imaging retinal pigment epithelial proliferation secondary to PASCAL photocoagulation in vivo by polarization-sensitive optical coherence tomography. *Am J Ophthalmol*. 2013;155:1058-1067e1051.

36. Tababat-Khani P, Berglund LM, Agardh CD, Gomez MF, Agardh E. Photocoagulation of human retinal pigment epithe- lial cells in vitro: evaluation of necrosis, apoptosis, cell migra- tion, cell proliferation and expression of tissue repairing and cytoprotective genes. *PLoS One*. 2013;8:e70465.

37. Lamouille S, Xu J, Derynck R. Molecular mechanisms of epithelial- mesenchymal transition. *Nat Rev Mol Cell Biol*. 2014;15:178-196.

38. Tamiya S, Liu L, Kaplan HJ. Epithelial-mesenchymal transition and proliferation of retinal pigment epithelial cells initiated upon loss of cell-cell contact. *Invest Ophthalmol Vis Sci*. 2010; 51:2755-2763.

39. Bakthisaran R, Tangirala R, Rao CM. Small heat shock  pro-  teins: role in cellular functions and pathology. *Biochim Biophys Acta*. 1854;2015:291-319.

40. Pichon S, Bryckaert M, Berrou E. Control of actin dynamics by p38 MAP kinase - Hsp27 distribution in the lamellipodium of smooth muscle cells. *J Cell Sci*. 2004;117:2569-2577.

41. Bruey JM, Ducasse C, Bonniaud P, et al. Hsp27 negatively reg- ulates cell death by interacting with cytochrome c. *Nat Cell Biol*. 2000;2:645-652.

42. Strunnikova N, Baffi J, Gonzalez A, Silk  W,  Cousins  SW, Csaky KG. Regulated heat shock  protein  27  expression  in human retinal pigment epithelium. *Invest Ophthalmol Vis Sci*. 2001;42:2130-2138.

43. Kannan R, Sreekumar PG, Hinton DR. Alpha crystallins in the retinal pigment epithelium and implications for the

pathogenesis and treatment of age-related macular degenera- tion. *Biochim Biophys Acta*. 1860;2016:258-268.

44. Nakata K, Crabb JW, Hollyfield JG. Crystallin distribution in Bruch's membrane-choroid complex from AMD and age- matched donor eyes. *Exp Eye Res*. 2005;80:821-826.

45. De S, Rabin DM, Salero E, Lederman PL, Temple S, Stern JH. Human retinal pigment epithelium cell changes and expression of alphaB-crystallin: a biomarker for retinal pigment epithe- lium cell change in age-related macular degeneration. *Arch Ophthalmol*. 2007;125:641-645.

46. Han L, Jiang Y, Han D, Tan W. Hsp27 regulates epithelial mes- enchymal transition, metastasis and proliferation in colorectal carcinoma. *Oncol Lett*. 2018;16:5309-5316.

47. Chen D, Cao G, Qiao C, Liu G, Zhou H, Liu Q. Alpha B- crystallin promotes the invasion and metastasis of gastric can- cer via NF-kappaB-induced epithelial-mesenchymal transition. *J Cell Mol Med*. 2018;22:3215-3222.

48. Gonzalez DM, Medici D. Signaling mechanisms of the epithelial-mesenchymal transition. *Sci Signal*. 2014;7:re8.

49. Ishikawa K, Sreekumar PG, Spee C, et al. alphaB-crystallin reg- ulates subretinal fibrosis by modulation of epithelial- mesenchymal transition. *Am J Pathol*.2016;186:859-873.

50. Kern K, Mertineit CL, Brinkmann R, Miura Y. Expression of heat shock protein 70 and cell death kinetics after different thermal impacts on cultured retinal pigment epithelial cells. *Exp Eye Res*. 2018;170:117-126.

51. Sramek C, Mackanos M, Spitler R, et al. Non-damaging retinal phototherapy: dynamic range of heat shock protein expression. *Invest Ophthalmol Vis Sci*.2011;52:1780-1787.

52. Lavinsky D, Wang J, Huie P, et al. Nondamaging retinal Laser therapy: rationale and applications to the macula. *Invest Ophthalmol Vis Sci*. 2016;57:2488-2500.

53. Michalczyk K, Ziman M. Nestin structure and predicted func- tion in cellular cytoskeletal organisation. *Histol Histopathol*. 2005;20:665-671.

54. Xue LP, Lu J, Cao Q, Hu S, Ding P, Ling EA. Muller glial cells express nestin coupled with glial fibrillary acidic protein in experimentally induced glaucoma in the rat retina. *Neurosci- ence*. 2006;139:723-732.

55. Engelhardt M, Bogdahn U, Aigner L. Adult retinal pigment epi- thelium cells express neural progenitor properties and the neuro- nal precursor protein doublecortin. *Brain Res*.2005;1040:98-111.

56. Chabot A, Hertig V, Boscher E, et al. Endothelial and epithelial cell transition to a mesenchymal phenotype was delineated by nestin expression. *J Cell Physiol*. 2016;231:1601-1610.

57. Zhang Y, Zeng S, Ma J, et al. Nestin overexpression in hepatocel- lular carcinoma associates with epithelial-mesenchymal transi- tion and chemoresistance.*J Exp Clin Cancer Res*. 2016;35:111.

58. Leopold PL, Vincent J, Wang H. A comparison of epithelial-to- mesenchymal transition and re-epithelialization. *Semin Cancer Biol*. 2012;22:471-483.

59. Baldin V, Lukas J, Marcote MJ, Pagano M, Draetta G. Cyclin D1 is a nuclear protein required for cell cycle progression in G1. *Genes Dev*. 1993;7:812-821.

60. Kim HD, Jang SY, Lee SH, et al. Retinal pigment epithelium responses to selective retina therapy in mouse eyes. *Invest Ophthalmol Vis Sci*. 2016;57:3486-3495.

61. Miura Y, Klettner A, Noelle B, Hasselbach H, Roider J. Change of morphological and functional characteristics of retinal pig- ment epithelium cells during cultivation of retinal pigment

epithelium-choroid perfusion tissue culture. *Ophthalmic Res*. 2010;43:122-133.

62. Jang SY, Cho IH, Yang JY, et al. The retinal pigment epithelial response after retinal laser photocoagulation in diabetic mice. *Lasers Med Sci*. 2019;34:179-190.

63. Gao H, Hollyfield JG. Aging of the human retina. Differential loss of neurons and retinal pigment epithelial cells. *Invest Ophthalmol Vis Sci*. 1992;33:1-17.

64. Starnes AC, Huisingh C, McGwin G Jr, et al. Multi-nucleate retinal pigment epithelium cells of the human macula exhibit a character- istic and highly specific distribution. *Vis Neurosci*. 2016;33:e001.

65. Stern J, Temple S. Retinal pigment epithelial cell proliferation. *Exp Biol Med (Maywood)*. 2015;240:1079-1086.

66. Chen M, Rajapakse D, Fraczek M, Luo C, Forrester JV, Xu H. Retinal pigment epithelial cell multinucleation in the aging eye—a mechanism to repair damage and maintain homo- eostasis. *Aging Cell*. 2016;15:436-445.

67. Yang JH, Yu SY, Kim TG, Kim ES, Kwak HW. Morphologic changes in the retina after selective retina therapy. *Graefes Arch Clin Exp Ophthalmol*. 2016;254:1099-1109.

68. Lavinsky D, Chalberg TW, Mandel Y, et al. Modulation of transgene expression in retinal gene therapy by selective laser treatment. *Invest Ophthalmol Vis Sci*. 2013;54:1873-1880.

69. Zhou M, Geathers JS, Grillo SL, et al. Role of epithelial- mesenchymal transition in retinal pigment epithelium dysfunc- tion. *Front Cell Dev Biol*. 2020;8:501.

70. The Macular Photocoagulation Study Group. Persistent and recurrent neovascularization after krypton laser photocoagula- tion for neovascular lesions of age-related macular degenera- tion. *Arch Ophthalmol*. 1990;108:825-831.

71. Owens SL, Bunce C, Brannon AJ, et al. Prophylactic laser treat- ment hastens choroidal neovascularization in unilateral age- related maculopathy: final results of the drusen laser study. *Am J Ophthalmol*. 2006;141:276-281.

72. Owens SL, Bunce C, Brannon AJ, Wormald R, Bird AC, Drusen Laser Study G. Prophylactic laser treatment appears to promote choroidal neovascularisation in high-risk ARM: results of an interim analysis. *Eye (Lond)*. 2003;17:623-627.

73. Findlay Q, Jobling AI, Vessey KA, et al. Prophylactic laser in age-related macular degeneration: the past, the present and the future. *Eye (Lond)*. 2018;32:972-980.

74. Sonoi R, Kim MH, Kino-Oka M. Facilitation of uniform matu- ration of human retinal pigment epithelial cells through collec- tive movement in culture. *J Biosci Bioeng*. 2016;121:220-226.

## SUPPORTING INFORMATION

Additional supporting information may be found online in the Supporting Information section at the end of this article.